# Corrosion of steel fibre reinforced concrete (SFRC) subjected to simulated stray direct (DC) interference

Kangkang Tang

kangkangtang@gmail.com (kangkangtang@gmail.com; kangkang.tang@brunel.ac.uk)

Brunel University London, Howell Building, Department of Civil and Environmenta, ~~UB8 3PN~~UB8 3PH, London, Uxbridge, United Kingdom

**Abstract**

Stray current induced corrosion is a major technical challenge for modern electrified railway systems. It can lead to corrosive damage to railway tunnel segmental linings and surrounding infrastructure. Steel fibre reinforced concrete (SFRC) represents a potential solution to this problem due to the possible lack of electrical continuity between steel fibres. Despite this potential advantage, there is still lack of knowledge concerning the susceptibility of SFRC to stray current induced corrosion. Instrumental methods for electrochemistry and computer simulations were conducted in this project to evaluate the corrosion susceptibility of SFRC under a simulated stray direct current (DC) condition. Results indicate that steel fibres have high inherent corrosion resistance to the stray DC interference under a chloride-free condition. The presence of a small amount of NaCl however can lead to enhanced stray DC-induced corrosion.

**Keywords:** Steel fibre reinforced concrete; Tafel polarization; EIS; Cyclic voltammetry; Passivity; Pitting corrosion; Boundary element method

## Nomenclature

$A$

Exposed anode area ($cm^2$)

$\beta_a$, $\beta_b$

Anodic and cathodic Tafel constants/gradients

$C_f$

Steel passive layer capacitance CPE ($S \bullet s^n cm^{-2}$)

$C_{dl}$

Double layer capacitance CPE ($S \bullet s^n cm^{-2}$)

$CR$

Corrosion rate (mm/year)

$E_{corr}$

Corrosion potential (V)

$I$

Measured current from the circuit or the net electron flow (A)

$I_{total}$

Total stray current (A)

$I_a$, $I_c$

Anodic and cathodic currents (A)

$I_{corr}$

Corrosion current (A)

$i_{corr}$

Corrosion current density (A/cm$^2$)

$L$

Distance between substations (km)

$\eta_{e,a}$, $\eta_{e,c}$

Anodic and cathodic overpotentials (V) from $Ee,a$ and $Ee,c$

$r_R$

Resistance of the running tracks (Ω/km)

$r_T$

Track-earth resistance (Ω•km)

$R_S$

Resistance of the solution (kΩ•cm$^2$ or kΩ)

$R_f$

Membrane resistance (kΩ•cm$^2$ or kΩ)

$R_{ct}$

Charge transfer resistance of the steel (kΩ•cm$^2$ or kΩ)

$R_p$

Linear polarization resistance (kΩ•cm$^2$ or kΩ)

$\theta$

Phase shift (radian)

# 1 Introduction

For an electrified railway, the transmission of power is normally provided by an overhead wire or a conductor rail. The return circuit is usually through the running tracks which are connected to nearby substations. Stray current refers to the electric current which disperses directly into the ground which performs as an unintended parallel return path. The leakage of stray current to surrounding structures, e.g. tunnel lining segments and reinforced concrete sleepers, can lead to steel reinforcement corrosion and the disintegration of concrete [1]. Stray current can also accelerate corrosion of neighbouring infrastructure such as underground service cables, water mains and gas pipes which will ultimately reduce their service life. The corrosive damage due to stray current will become more prominent in the UK as the government is committed to developing more electrified rail networks to provide sustainable and cleaner services for the public (an electric train consumes 20% less power compared to a diesel-powered train, along with a reduced $CO_2$ emission by at least 20% [2]). This includes major work for the £15 billion Crossrail project

and the construction of the £56 billion High-Speed 2 (HS2) project. As a result, the prevention and mitigation of stray current induced corrosion will form an important element of the design, construction and operation of the electrified railway systems. Steel fibre reinforced concrete (SFRC) represents a potential solution to this problem. ACI report number 544 [3] on the physical properties and durability of fibre-reinforced concrete states that "*since the fibres are short, discontinuous and rarely touch each other, there is no continuous conductive path for stray or induced currents or currents from electromotive potential between different areas of the concrete*". Based on this information, SFRC is an ideal substitute for conventional steel reinforcement in electrified railway, with less concern about stray current induced corrosion. From a structural perspective, the compressive strength of a railway tunnel is of the upmost importance to ensure its overall stability. SFRC has a high compressive strength and better fire resistance in comparison to that of ordinary steel reinforced concrete [4,5]. All these make railway tunnel lining construction a favoured application of SFRC. Despite these advantages, there is still lack of knowledge concerning the susceptibility of stray current induced corrosion of SFRC and no recognised methodology that is suitable to assess it.

Corrosion of conventional steel reinforcement is often of an electrochemical nature, consisting of at least two half-cell reactions, i.e. an oxidation reaction at an anode (loss of electron) and a reduction reaction at a cathode (gain of electron). Coupled anodic and cathodic reactions can cause a small transient in the electric charges. Steel corrosion or oxidization is the result of these electric charges according to Faraday's laws of electrolysis: the amount of substance which reacts or liberates is directly proportional to the quantity of electric charges passing through it. The steel corrosion rate can be evaluated by conducting a Tafel polarization test. A nonlinear regression analysis can be conducted to determine $I_{corr}$ based on Butler-Volmer equation (Eq. (1)).

$$I = I_{corr}\left[\exp\left(\frac{\mathrm{E}-E_{corr}}{\beta_a}\right) - \exp\left(-\frac{\mathrm{E}-E_{corr}}{\beta_c}\right)\right] \quad \textbf{(1)}$$

$E$ represents the amplitude of the DC voltage (V); $I$ represents the net electron flow (A) obtained in the working electrode. In addition to $I_{corr}$, anodic and cathodic Tafel constants ($\beta_a$, $\beta_b$) can be determined through the regression analysis. In comparison to the Tafel polarization test, a small DC or AC voltage perturbation, e.g. ± 20 mV (vs OCP), is required for the linear polarization resistance (LPR) test and the Electrochemical Impedance Spectroscopy (EIS) test. On the other hand, important kinetic parameters such as $\beta_a$ and $\beta_b$ cannot be determined through either LPR or EIS test due to the small range of voltage perturbation applied.

In addition to an external DC voltage ($E$), the presence of chloride in concrete, which can be a result of contaminated aggregate or mixing water, can lead to serious localized corrosion or pitting corrosion by breaking down the steel passive layer [6]. This detrimental effect was described by Saremi et al. [7] as a competing process between hydroxide and chloride ions which coexist in the concrete pore solution: pitting only occurs when the disruptive effect of chloride ions overcomes the effect of hydroxide ions which stabilize the surface lattice of steel. Steel reinforcement is susceptible to corrosion when the chloride content exceeds a chloride threshold level, e.g. 0.4% (by mass of cement) for building structures [8] and a more stringently 0.2% for bridges [9]. Hausmann [10] suggested a chloride threshold level of 0.61 based on a free [$Cl^-$~~]/[OH-~~/[$OH^-$] ratio, i.e. the ratio of the free chloride concentration to that of the hydroxide ions in the concrete pore solution. In comparison to the chloride threshold defined by mass of cement, a [$Cl^-$~~]/[OH-~~/[$OH^-$] threshold ratio can better consider the effect of hydroxide ions which is related to the passivation of a steel reinforcement.

The chloride threshold of steel fibres was found to be much higher that of conventional steel reinforcement. For instance, Mangat and Gurusamy [11] reported that the chloride threshold for corrosion of steel fibres with a diameter between 0.99 and 1.18 mm was one order of magnitude higher than that of a steel reinforcing bar. A [$Cl^-$~~]/[OH-~~/[$OH^-$] ratio above 0.61, i.e. the chloride threshold for ordinary steel reinforced concrete, did not lead to any corrosive attack to the embedded steel fibres at a depth of 30 mm into a SFRC specimen after a simulated marine exposure for 1250 days [11]. All these indicate that SFRC has a better ability to withstand chloride attack in comparison to that of ordinary steel reinforcement. It should be noted that chloride exists in two different forms in concrete, i.e. free and bound chloride. Bound chloride is chemically or physically attached to the cement hydration products; only free chloride ions in the concrete pore solution are responsible for the depassivation of steel reinforcement [12]. As bound chloride can be released into the concrete pore solution due to a reduction in pH, it is important to consider the effect of pH when determining the chloride threshold for the corrosion of steel reinforcement [8,13].

Concrete has high pH (≥ 12) and its porous structure allows ions (e.g. $OH^-$~~ and Cl-~~ and $Cl^-$) and molecules (e.g. $O_2$) to get in contact with steel. Based on a review of the literature, alkaline solutions such as a saturated solution of calcium hydroxide has be used to simulate the concrete pore solution in the study of the corrosion behaviour of steel reinforcement [4,14–18]. The effect of chloride can be considered by adding NaCl into the simulated concrete pore solution [16,19]. This has been followed in this work and NaCl was added into the simulated concrete pore solutions at different concentrations to simulate different working conditions, e.g. from a chloride free condition to a marine environment. It should be noted that the chloride threshold determined in concrete was reported to be much higher than that determined using a simulated concrete pore solution [20]. Page [~~20~~20] attributed such enhanced steel corrosion resistance to the buffering effect of the cement paste layer precipitated on the steel surface. There is therefore scope to justify the results, e.g. steel corrosion data, obtained using a simulated concrete pore solution by conducting a comparison study using a solid electrolyte such as concrete.

An externally applied potential ($E$), as experienced by a railway tunnel to a stray DC current, can push the anodic potential away from the equilibrium state and accelerate the anodic reaction. Based on a review of the literature, the effect of a stray DC current has been simulated by applying either a controlled electric voltage (potentiostatic) or current (galvanostatic) [21–24]. The potentiostatic polarization technique allows a constant DC voltage to be applied to a metal sample while the current flow is measured. For instance, Wang et al. [24] investigated the corrosion fatigue effect of reinforced concrete beams subjected to a 30 V DC voltage which simulated the stray DC

environment. Previous investigations [4] however indicate that corrosion potential ($E_{corr}$) may vary when the working electrode (e.g. steel) is pre-exposed to a stray current interference. This indicates that maintaining the same external voltage ($E$) over a long period of time may not necessarily ensure that the same form (anodic or cathodic) and intensity of a stray DC interference. In comparison to the potentiostatic polarization technique, a galvanostatic (controlled electric current) polarization technique can better represent a stray current effect. This is also according to Niasati and Gholami's electric circuit model, which is schematically shown in Fig. 1, to determine the stray current:

$$i_S = \frac{R_R i_T}{R_T + R_R + R_{soil}} \quad \textbf{(2)}$$

$i_S$ represents the stray current (A); $i_T$ represents the railway traction current (A); $R_R$ represents running rail resistance (Ω•m); $R_{soil}$ and $R_T$ represents soil and track-and-earth resistance (Ω•m). A standard track-and-earth insulation, complying with EN 50122-2 [31], can maintain constant track-and-earth resistance ($R_T$). Running rail resistance ($R_R$) can also be maintained due to a constant spacing, e.g. 2 km is normally adopted between substations by DC railway systems [25]. It is therefore sufficient to justify that a linear correlation between $i_S$ and $i_T$ for a given length of railway between substations and a given value of resistance between the track and earth. It is also a logical way to simulate a stray DC environment by controlling the stray current value. Charalambous et al. [26] reported that a stray current of 50 mA was measured in a railway transit system under a traction current of 1000 A ($i_T$). This has been followed in this work and a constant DC current up to 50 mA was used to simulate the stray current arising from an electrified railway. This is detailed in Section 2.2.

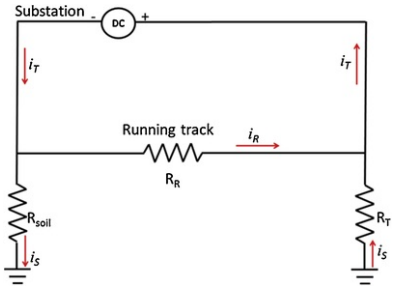


**Fig. 1** Equivalent electronic circuit modelling the formation of stray current ($i_S$).

alt-text: Fig. 1

In addition to electrochemical and electrical analyses discussed above, numerical analysis based on finite element method (FEM) and boundary element method (BEM) has been increasingly used in the study of corrosion behaviour of steel reinforcement. For instance, Laurens et al. [27] investigated macrocell corrosion in steel reinforced concrete based on FEM modelling. The polarization behaviour of steel reinforcement (i.e. $E$-$I$ curves) was defined by maintaining constant polarization parameters (e.g. $\beta_a$ and $\beta_c$). This steady-state analytical approach was based on the assumption that both anodic and cathodic reactions are kinetically controlled. In comparison to FEM, BEM only needs to discretize active boundaries and this can greatly improve the modelling efficiency. Cui et al. [28] investigated stray DC-induced corrosion in a 1.6 km pipeline through BEM modelling. Only the pipeline (i.e. the active boundary) was discretized which greatly reduced the total number of elements needed for meshing surrounding soil. In this work, numerical modelling based on BEM modelling was carried out to investigate the corrosion behaviour of SFRC subjected to a simulated stray DC interference. This is discussed in Section 2.3.

# 2 Experimental and analytical procedures

The primary objective of this work was to compare different instrumental methods in electrochemistry for the assessment of the corrosion behaviour of steel fibre which has great potential to replace conventional steel reinforcement in railway tunnel construction. These experimental methods include Tafel polarization, Linear Polarization Resistance (LPR), Cyclic Potentiodynamic (CP) polarization and Electrochemical Impedance Spectroscopy (EIS). Another objective of this work was to determine whether a stray direct current (DC) can be picked up and transferred by discontinuous steel fibres, if so, to quantify under what circumstances this might occur. This was conducted through the stray DC interference test as discussed in Section 2.2 and BEM modelling as discussed in Section 2.3.

As discussed in Section 1, an aqueous electrolyte based on the saturated calcium hydroxide solutions is cost effective, environmental friendly and easier to prepare in comparison to a solid electrolyte (e.g. concrete) in the study of steel reinforcement corrosion. This has been followed in this work and reagent grade NaCl was added into the simulated pore solution at different concentrations (0.0, 0.3, 0.6 and 0.8 mol/L or M), representing different working conditions from a chloride free condition to a marine environment [19]. In order to verify that the results obtained using simulated concrete pore solutions were still applicable for SFRC, a comparison study using mortar as a solid electrolyte was conducted and this is discussed in Section 2.2.2.

A TAS environmental chamber was used as a Faraday cage, inside which the electrochemical tests discussed in this work were conducted. The exterior and interior parts of the environmental chamber are made from stainless

steel and connected to earth to protect the interior from the outside electromagnetic interference, e.g. fluorescent lighting and mobile communication devices. The corrosion of SFRC under an externally DC voltage may also be affected by the rate of mass transport or diffusion which changes along with the ambient temperature variations. The environmental chamber was set at a constant temperature (20 °C) and humidity (90%), ensuring the reproducibility and repeatability of the experimental results.

## 2.1 Corrosion behaviours of steel fibres

### *2.1.1 Tafel polarization test*

The steel fibre used in this work (Fig. 2) was provided in bags by Bekaert. These cold drawn low carbon steel fibres, 62 mm in length and 0.75 mm in diameter, have deformed ends and were adhered together by water reactive glue to facilitate concrete mixing. Steel fibres were flushed with deionized water to remove the water-soluble adhesive prior to testing. A 3-electrode electrochemical cell (Fig. 3) was developed for the Tafel polarization test. A steel fibre (Fig. 2) was used as the working electrode (WE). It gives an exposed area of 1.4 $cm^2$ to the electrolyte. The permeation property and porous structure of concrete was simulated using a high density upholstery foam beam, soaking up the simulated pore solution. The porous structure of the foam beam allows ions (e.g. $OH^-$ ~~and Cl-~~ and $Cl^-$) and $O_2$ molecules in the electrolyte to reach the WE. The electrode potential of the working electrode was measured against a silver/silver chloride (Ag/AgCl) reference electrode (RE, with filling solution 3% KCl) which was placed on the top surface of the foam beam. Open circuit potential (OCP) represents a constant offset potential between the working electrode (WE) and counter electrode (CE). A conditioning time of 15 min~~utes~~ was maintained for all tests and the OCP was determined when a drift rate less than 0.05 mV/sec was achieved. During Tafel polarization, a DC potential perturbation, ±250 mV (vs OCP), was applied to the WE at a potential scanning rate of 1 mV/sec. The current flow between the WE and a 40 × 50 × 3 mm graphite counter electrode (CE) was measured by a Gamry Interface 1000E potentiostat. To study the effect of chloride ions on the corrosion behaviour of steel fibres, reagent grade NaCl was added into the simulated concrete pore solution at different concentrations, i.e. 0.0, 0.3, 0.6 and 0.8 mol/L, representing different working conditions as discussed. Three parallel samples were prepared and tested in each group. Freshly prepared electrodes and electrolytes were used in each test. Tafel polarization results are discussed in Section 3.1.1.

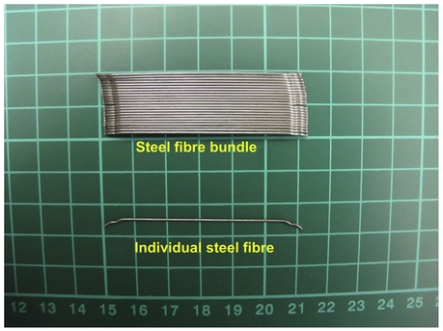


**Fig. 2** Steel fibre (DRAMIX 4D 80/60BG).

alt-text: Fig. 2

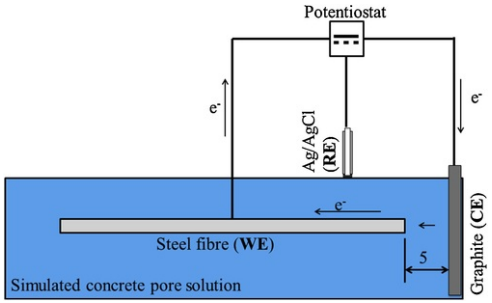


**Fig. 3** Tafel polarization test (all units in mm).

alt-text: Fig. 3

The pH of the concrete pore solutions was assessed using a Phidget pH sensor and results are shown in Fig. 4. pH was found to range between 11.2 and 12.6. The latter is similar to that reported for ordinary steel reinforced concrete, i.e. about

12.5 [4]. pH of the simulated concrete pore solutions containing NaCl was less than 12, which might be attributed to the 'alkaline error' of the glass pH electrode [29].

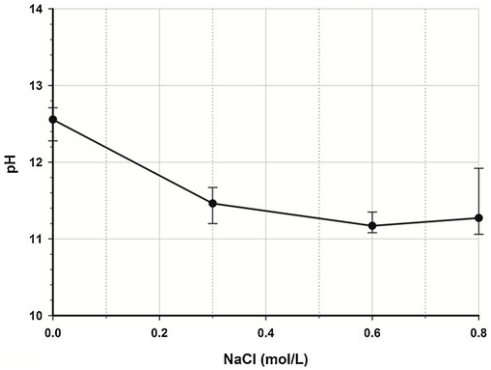


**Fig. 4** pH of simulated concrete pore solutions.

alt-text: Fig. 4

### *2.1.2 Linear polarization resistance (LPR) test*

The same 3-electrode electrochemical cell (Fig. 3) was used for the LPR test. In comparison to the Tafel polarization technique, only a small DC perturbation, e.g. ± 20 mV from the open circuit potential (OCP), is required. A reduced potential scanning rate of 0.2 mV/sec was adopted and this can better assess the linear correlation between the applied potential ($E$) and measured current ($I$). The polarization resistance, $R_p$, was determined as the tangent of the $E$-$I$ curve. A constant $B$ value of 26 mV was used for the calculation of corrosion density ($i_{corr}$) according to Eq. (3). As Tafel polarization and LPR tests may change the surface properties of steel fibres, fresh steel fibres, foam beams and electrolytes were prepared and used each time. Two parallel samples were prepared and tested in each group.

$$I_{corr} = \frac{B}{R_p} \quad \textbf{(3)}$$

### *2.1.3 Electrochemical impedance spectroscopy (EIS)*

EIS was conducted by sweeping a small sinusoidal voltage $E_0 \bullet \sin(\omega t)$ ( $E_0 = 25\,mV$ ) to the WE, at frequencies ( $\omega$ ) varying between $10^5$ and $10^{-1}$ Hz using the same electrochemical cell as that used in the Tafel polarization test (Fig. 3). The cell's current response was also sinusoidal but phase shifted ($\theta$), $I_0 \bullet \sin(\omega t + \theta)$ . The impedance of the electrochemical cell ($Z$) was determined as the correlation between the applied potential ($E$) and the measured current ($I$). The interpretation of EIS data was based on the best-fit results obtained through equivalent electrical circuit modelling. Three parallel samples were prepared and tested in each group. The EIS data provide quantitative information about the corrosion state of steel in concrete. This is discussed in Section 3.1.3.

### *2.1.4 Cyclic ~~P~~potentiodynamic (CP) polarization test*

The CP polarization test was conducted to obtain additional information about the passivation behaviour of steel fibres and the breakdown of the passive layer within the positive or anodic region. The same 3-electrode electrochemical cell (Fig. 3) was used for the CP polarization test. During CP polarization, the potential was applied against the Ag/AgCl RE placed on the top surface of the foam beam; the current flow between the WE and CE was measured by the Gamry potentiostat. CP polarization was obtained based on the potential sweep mainly along the positive or anodic direction, e.g. -0.5 to 1.5 V from the OCP, at a scanning rate of 5 mV/sec. A reverse scan was only conducted when either the maximum potential (i.e. 1.5 V vs OCP) or a maximum current density of 30 mA/cm$^2$ was reached. The maximum current density was adopted to avoid overloading and damaging the potentiostat. One sample was prepared and tested in each group. Freshly prepared electrodes and electrolytes were used in each test. CP polarization provides useful information about the steel pitting potential ($E_{pit}$) and peak current density ($i_{peak}$) which can be used to quantitatively assess the corrosion susceptibility of steel fibre subjected to an external DC voltage. This is discussed in Section 3.1.4.

## 2.2 Investigation of stray DC-induced corrosion in SFRC subjected to a simulated stray current interference

### *2.2.1 Stray DC interference test – use of simulated concrete pore solutions*

Fig. 5 shows the experimental setup of the stray DC interference test. A controlled DC current of 50 mA was maintained between two graphite auxiliary electrodes (40 × 50 × 3 mm) to simulate the effect of a stray DC interference from an electrified railway. This was according to the published data by Charalambous et al. [26] who reported a stray current up to 50 mA along a railway line despite that high track-and-earth resistance ($R_T$) of 100 Ω•km has been achieved. A steel fibre was placed between two graphite plates with a gap of 5 mm to simulate the discontinuous nature of steel fibres in a SFRC segmental lining. The graphite electrodes and steel fibre were embedded into a high density upholstery foam beam, soaking up the simulated concrete pore solution to simulate the porous structure of a concrete segmental lining. A 20-min 50 mA stray DC interference test was conducted using the Gamry Interface 1000E potentiostat with the Gamry's Virtual Front Panel (VFP600) software package which allows the voltage drop between the embedded steel fibre and the auxiliary graphite electrode to be measured in the meanwhile. This allows for the justification of whether a discrete steel fibre can pick up and transfer a stray DC current. Freshly prepared electrodes and electrolytes were prepared at the start of each test. Two parallel samples were prepared and tested for each simulated concrete pore solution containing 0.0 or 0.3 mol/L NaCl. After the simulated stray DC interference, a Tafel polarization test was conducted following the same procedure as discussed in Section 2.1.1 using a freshly prepared saturated calcium hydroxide solution as the electrolyte. Tafel slope analysis was then conducted to determine the corrosion current density ($i_{corr}$) and corrosion potential ($E_{corr}$). Results are discussed in Section 3.2.1.

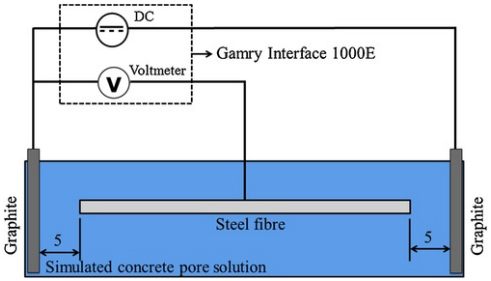


**Fig. 5** Stray DC interference test (20-min 50 mA).

alt-text: Fig. 5

## 2.2.2 Stray DC interference test – corrosion measurement in SFRC

The electrical resistance and electronic structures of an aqueous electrolyte is often different from a solid electrolyte such as concrete, even with similar chemical compositions [4,30]. In order to verify that the results obtained using aqueous electrolytes were applicable for SFRC, a 3-electrode electrochemical cell, as seen in Fig. 6, was developed but using mortar as the electrolyte. Mortar is a mixture of cement, water and sand and the mix proportions used are shown in Table 1. The cement used for this project was CEM I 52,5 and the fine aggregate was well-graded medium sand with a water absorption value of 2.62%. 9 mortar specimens, 50 × 50 × 50 mm, were cast from the same batch of mortar used in the electrochemical cell. Within 24 h~~ours~~ of casting, these mortar cube specimens were demoulded and placed into a water curing tank which was set at 20 °C. The conformity of mortar properties was checked through the compressive strength test conducted at the age of 3, 7 and 28 days after casting. Fig. 7 shows that a very consistent compressive strength has been achieved at different ages, indicating a good quality control during the casting and curing processes.

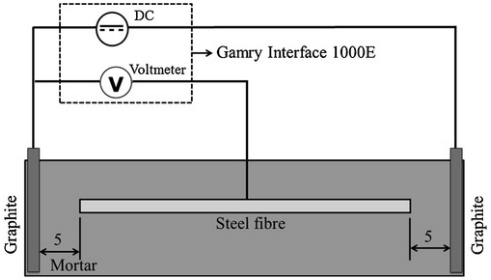


**Fig. 6** Stray DC interference test (1-hr 30 mA).

alt-text: Fig. 6

**Table 1** Mortar mix proportions.

alt-text: Table 1

| Mortar mixes | CEM I 52,5 (kg/m³) | Free W/C | Sand (0-4 mm) ~~(kg/m3)NaCl~~(kg/m³) | NaCl (kg/m³) |
|---|---|---|---|---|

| | | | | |
|---|---|---|---|---|
| 0%NaCl | 480 | 0.35 | 1814 | 0 |
| 2%NaCl | 480 | 0.35 | 1814 | 9.6 |

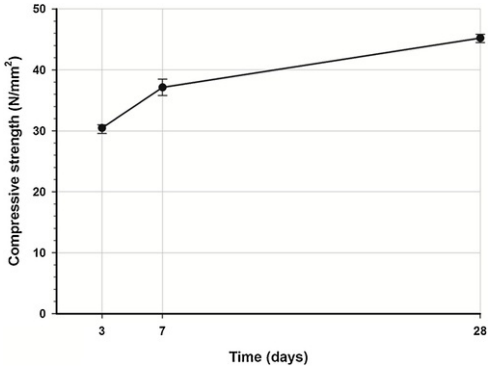


**Fig. 7** Mortar compressive strength at the age of 3, 7 and 28 days (verification of conformity).

alt-text: Fig. 7

The effect of chloride ions on the corrosion behaviour of SFRC was investigated by adding 0 or 2% NaCl (by mass of cement) into the mortar mixes. Two parallel samples were prepared in each mix. A steel fibre, connected to a copper cable and coated with hot melt polymer adhesive, was embedded into the fresh mortar mix. It also gives an exposed area of approximate 1.4 $cm^2$ of the steel fibre to the electrolyte. All mortar specimens were placed in the environmental chamber set at 20 °C and 90% humidity after casting. The stray DC interference test was conducted at the age of 3 days after casting. A controlled DC current of 30 mA was used to simulate the stray DC interference due to the high impedance of mortar which needs a high voltage to push the DC current through. The direct current (DC) perturbation was maintained between two graphite auxiliary plates, 40 × 50 × 3 mm, for 1 hour. In the meanwhile, the voltage drop between the steel fibre and the graphite electrode was monitored by the Gamry Interface 1000E potentiostat. After the 1-hr DC interference, EIS was conducted to determine the corrosion behaviour of the embedded steel fibre following the similar procedure as discussed in Section 2.1.3. The embedded steel fibre was used as the working electrode (WE) and both graphite plates were used as the counter electrode (CE) to close the electric circuit required for the EIS measurement, as seen in Fig. 8. An Ag/AgCl reference electrode (RE) was placed on the top surface of the mortar via a sponge soaking saturated $Ca(OH)_2$ solution to determine the electrode potential. The interpretation of EIS data was based on the best-fit results obtained through equivalent electrical circuit modelling and this is discussed in Section 3.2.2.

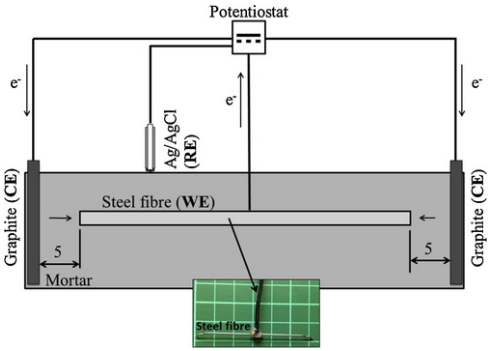


**Fig. 8** SFRC EIS test.

alt-text: Fig. 8

## 2.3 Boundary element method (BEM) modelling

The developed electric potential ($E$) in an energy conserved system is governed by Laplace equation (Eq. (4)).

$$\nabla^2 (E) = 0 \quad \textbf{(4)}$$

In a two dimensional coordinate system, Eq. (4) can be written as Eq. (5).

$$\nabla^2(E) = \frac{\partial^2 E}{\partial x^2} + \frac{\partial^2 E}{\partial y^2} = 0 \quad \textbf{(5)}$$

The numerical solution of Eq. (4) or (5) through FEM or BEM approaches, considering the initial boundary conditions, will provide information such as the current distribution in an electrolyte domain. In this study, numerical modelling based on the boundary element method (BEM) was conducted using COMSOL Multiphysics 5.4. Only the "active" domains, i.e. electrodes and steel fibre, were discretized and this greatly reduced the total number of elements and nodes needed for the electrolyte. As shown in Fig. 9, this is a 2D semi-infinite model with its top surface in contact with air. Both auxiliary graphite electrodes and the embedded steel fibre were meshed into 1D pipe elements which allow for identical electrical potential around the element circumference [28,31]. The steel polarization curves (or $E$-$I$ curves) were considered based upon a piecewise linear interpolation approach [28], i.e. the nonlinear polarization curves were represented as a number of straight lines (Fig. 10) which approximates the kinetics of electrochemical reactions occurring at the steel-electrolyte interfaces. A DC current of 50 mA, same as that used in the stray DC interference test (Section 2.2.1), was applied between two graphite electrodes. As the current distribution in the BEM model still complies with the Ohm's law, the electrical conductivity (S/m) of the electrolyte was assumed uniform. Two electrolytes, which were same as those used in the stray DC interference test (Section 2.2.1), were considered in the BEM modelling: 1) saturated calcium hydroxide solution containing 0.0 mol/L NaCl and 2) saturated calcium hydroxide with 0.30 mol/L NaCl. Their electrical conductivities were respectively taken as 0.73 and 2.4 S/m according to published experimental data [32,33]. The BEM modelling results are discussed in Section 3.3.

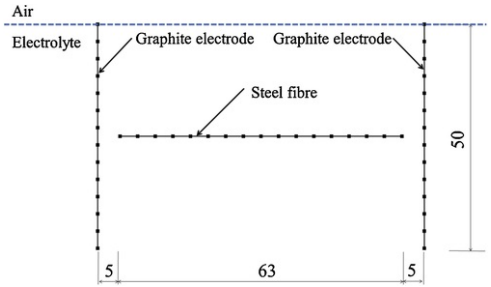


**Fig. 9** BEM model (all units in mm).

alt-text: Fig. 9

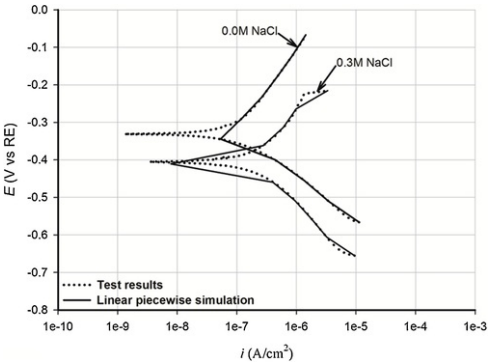


**Fig. 10** Linear piecewise simulation of polarization ($E$-$I$, $E$-$i$) curves in BEM modelling.

alt-text: Fig. 10

# 3 Results and discussion

## 3.1 Corrosion behaviour of steel fibres

### *3.1.1 Tafel polarization results*

Three instrumental methods for electrochemistry including Tafel polarization, LPR and EIS techniques were conducted to determine the corrosion current density ($i_{corr}$) of steel fibres under different chloride ion concentrations, upon which the corrosion resistance of steel fibres could be evaluated. The Tafel polarization results are presented as curves between the electrode potential $E$ (vs RE) and the total current density $i$ ($i = I / A$) on a logarithmic scale (Fig. 11). $A$ represents the exposed surface area of the steel fibre to the foam beam, i.e. 1.4 $cm^2$. A nonlinear regression analysis based on Butler-Volmeter equation (Eq. (1)) was conducted to determine $i_{corr}$ and the corrosion potential ($E_{corr}$) using Gamry Echem Analyst software [34].

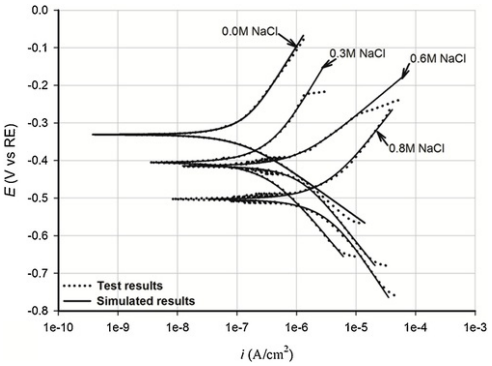


**Fig. 11** Tafel polarization results (before pre-exposure to a DC current).

alt-text: Fig. 11

The best-fit results for $i_{corr}$ and $E_{corr}$ are presented in Fig. 12. It shows that $E_{corr}$ reduced with an increase of chloride concentrations and this agrees with the previous research for ordinary steel reinforced concrete [35]. $i_{corr}$ obtained at a chloride concentration of 0.6 mol/L, which is similar to the salinity of seawater, was still less than 0.8 μA/$cm^2$, indicating high corrosion resistance. This is despite that a notable decrease in $E_{corr}$ from −360 mV to −480 mV (vs RE) with 0.6 mol/L chloride ions in the electrolyte. As the corrosion rate ($CR$) is proportional to $i_{corr}$, an assessment for the corrosion severity based on $E_{corr}$ values only may lead to a biased result.

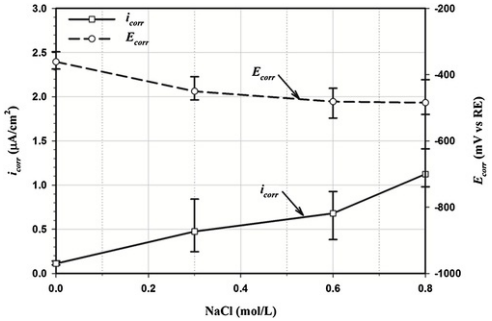


**Fig. 12** Tafel polarization results ($i_{corr}$ and $E_{corr}$).

alt-text: Fig. 12

## 3.1.2 LPR results

The polarization resistance, $R_p$, was determined as the tangent of the $E$-$I$ curves (Fig. 13) near the open circuit potential (OCP), e.g. ± 20 mV. $i_{corr}$ was calculated according to Stern-Geary equation (Eq. (3)) based on a constant $B$ value of 26 mV [36]. The average value obtained from two parallel samples are shown in Fig. 14. It shows that $R_p$ maintained constantly with up to 0.3 mol/L NaCl added into the electrolyte. A higher content of chloride ions (≥ 0.6 mol/L) shifted $E$-$i$ curves to more negative values in conjunction with a reduced $E$-$I$ slope or $R_p$. In comparison to $i_{corr}$ obtained through Butler-Volmer regression analysis (Fig. 12), Eq. (3) based on the LPR test led to a reduced $i_{corr}$, especially for high chloride concentrations (i.e. 0.6 and 0.8 mol/L). Stern-Geary equation (Eq. (3)) is a mathematically reduced form of Butler-Volmeter equation (Eq. (1)) with a constant $B$ value representing the effect of Tafel coefficients $\beta_a$ and $\beta_c$ [37]:

$$B = \frac{\beta_a \beta_c}{\beta_a + \beta_c} \quad \textbf{(6)}$$

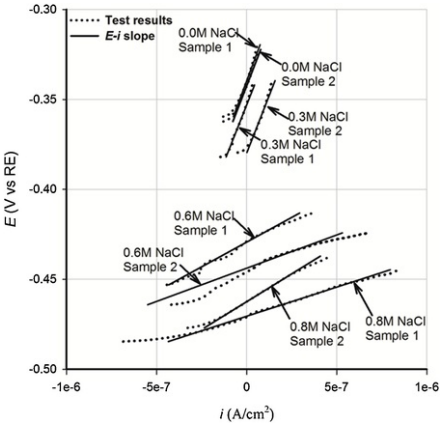


**Fig. 13** LPR test results (before pre-exposure to a DC current).

alt-text: Fig. 13

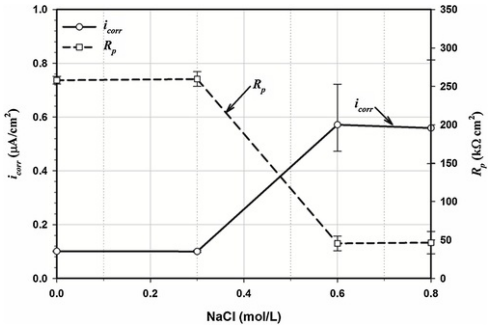


**Fig. 14** $i_{corr}$ determined based on LPR results.

~~(a) Bode phase plot~~

~~(b) Bode |Z| plot~~

~~(c) Nyquist plot~~

alt-text: Fig. 14

LPR is obtained through a linear potential sweep near the OCP (e.g. ± 20 mV) but $\beta_a$ and $\beta_c$ define the *E-I* curves at a larger overpotential value from OCP (e.g. ± 250 mV). It may lead to an intrinsic error in Eq. (3) by maintaining a constant $B$ (e.g. 26 mV) value when calculating $i_{corr}$. This is an area where ongoing research is undertaken.

### *3.1.3 EIS results*

EIS was conducted by applying a small sinusoidal potential to the electrochemical cell while its current response was recorded by the potentiostat. EIS data were first validated through a Kronig-Kramers (K-K) analysis using Gamry Echem Analyst software which showed that the whole system was causal and stable [34]. EIS data obtained from one sample in each group were presented as the Bode phase plot (Fig. 15(a)), Bode $|Z|$ plot (Fig. 15(b)) and Nyquist plot (Fig. 15(c)). The Bode phase plot allows the phase shift angle ($\theta$) to be plotted with regards to the excitation frequency (Hz) on a logarithmic scale. The Bode $|Z|$ plot allows the absolute values of the impedance ( $|Z|$ ) to be plotted against the logarithm of frequency (Hz). The Nyquist plot (Fig. 15(c)) allows the imaginary resistance ( $Z''$ ) to be plotted against the real resistance ( $Z'$ ). Each dot in the Nyquist plot represents the impedance measured at an excitation frequency. The Nyquist plot allows the impedance data to be discussed at high and low frequencies: the transfer resistance dominates at high frequencies and diffusion or mass transfer determines at low frequencies [38]. The correlations between $|Z|$, $Z'$, $Z''$ and $\theta$ are defined by Eq. (7) and (8).

$$|Z| = \sqrt{(Z')^2 + (Z'')^2} \quad \textbf{(7)}$$

$$\tan\theta = \frac{Z''}{Z'} \quad \textbf{(8)}$$

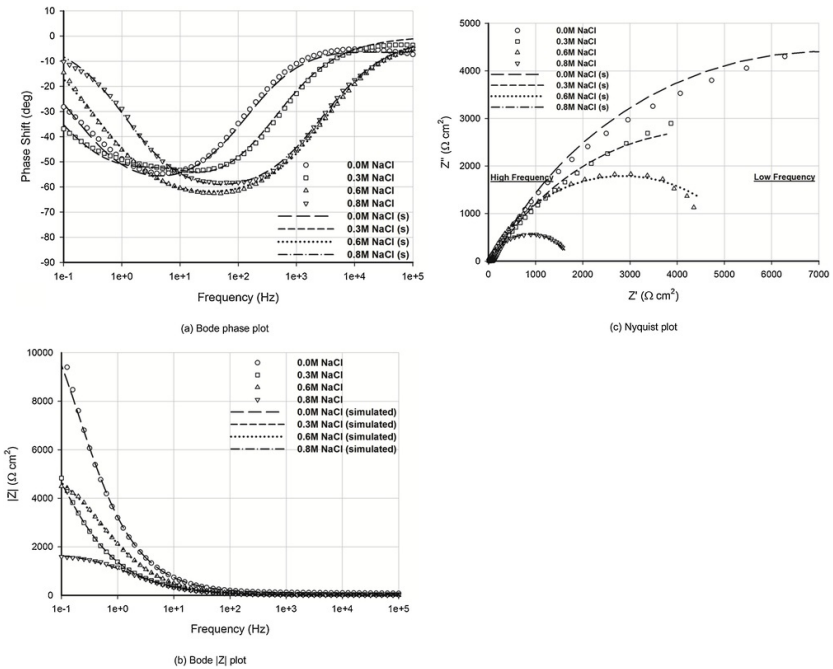


**Fig. 15** EIS data and best fit curves results (before pre-exposure to a DC current).

alt-text: Fig. 15

EIS data provide useful information about the steel passive layer properties (at low frequencies) and the dielectric properties of the steel-concrete interface (at high frequencies). The Bode phase plot (Fig. 15(a)) shows that the phase angle ($\theta$) dropped gradually at low frequencies between 0.1 and 100 Hz in a chloride-free environment. This indicates that the steel passive layer might have been locally destroyed or pitting corrosion has already occurred [35]. With 0.3 mol/L NaCl in the electrolyte, the phase angle ($\theta$) dropped constantly at low frequencies until the lowest value (valley) was reached at an excitation frequency of approximate 10 Hz, indicating the rate of charge transfer increased and the mass transfer might have become a key parameter governing the corrosion rate. With 0.6 and 0.8 mol/L NaCl in the electrolyte, $\theta$ dropped constantly at low frequencies until the lowest value (valley) was reached at an excitation frequency of approximate 100 Hz. A rust layer might have formed on the steel fibre surface and the speed of the corrosion reactions was governed by the diffusion speed through the rust layer in such circumstances [35].

The Bode $|Z|$ plot (Fig. 15(b)) shows that $|Z|$ dropped significantly from around 10,000 Ω•cm$^2$ at an excitation frequency of 0.1 Hz to less than 30 Ω•cm$^2$ at $10^5$ Hz. $|Z|$ obtained at the high frequency represents the bulk resistance of the solution ($R_s$) which is much smaller than the charge transfer resistance ($R_{ct}$). This finding also agrees with the Nyquist plot (Fig. 15(c)): the real impedance ( $Z'$ ) within the high frequency region ($10^5$ Hz) was found to be less than 30 Ω•cm$^2$ and this could be attributed to the small resistance of the aqueous electrolyte used.

An equivalent circuit (Fig. 16) was proposed to represent the corrosion state experienced by the steel fibre as discussed above. The solution resistance was represented as $R_s$. The membrane resistance ($R_f$) and charge transfer resistance ($R_{ct}$) were introduced into the circuit to represent the resistance of the passive layer and the charge transfer resistance of the electrode-electrolyte interface. $R_{ct}$ and $R_f$ define the difficulty of a kinetically controlled electrochemical process. The capacitance of the steel passive layer was represented by a capacitor ($C_f$) in the electronic circuit. The electrical double layer between the electrode and electrolyte was modelled as a capacitor ($C_{dl}$) too. A constant phase element (CPE), rather than a standard capacitor, was used in the equivalent circuits to model $C_f$ and $C_{dl}$, as it can better model the surface roughness and heterogeneousness of a double layer [14]. The impedance of a CPE can be defined as:

$$Z(\omega) = \frac{1}{Q}(j\omega)^{-n} \quad \textbf{(9)}$$

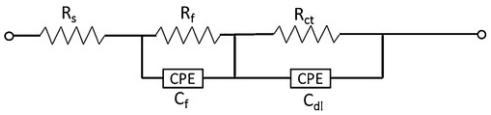


**Fig. 16** Equivalent circuit model.

alt-text: Fig. 16

$Q$ is a constant and $n = 1$ represents a perfect capacitor. Best-fit curves based on the equivalent electronic circuit modelling were obtained using Gamry Echem Analyst software [34] and they match very well with the original EIS data shown in Fig. 15. EIS best-fit results are presented in Table 2 based on the average results obtained from three parallel samples in each group. The presence of NaCl in the electrolyte reduced both $R_{ct}$ and $R_s$. $R_{ct}$ reduced by almost one degree of magnitude from 15.0 to 2.4 kΩ•cm$^2$, with 0.8 mol/L NaCl added into the electrolyte and this shows high corrosion susceptibility. Table 2 also shows that $R_f$ is much smaller than $R_{ct}$ and this can be attributed to the chloride induced depassivation effect [14]. In addition to $R_{ct}$ and $R_f$, a significant increase of $C_{dl}$ ($\geq 85 \times 10^{-6}$ S•s$^n$ cm$^{-2}$) was identified at high NaCl concentrations, i.e. 0.6 and 0.8 mol/L. This indicates that generalized corrosion had occurred on the steel fibre surface [7,14]. $R_{ct}$ was found to be lower than the polarization resistance ($R_p$) obtained through the LPR technique as shown in Fig. 14. As a result, corrosion current densities ($i_{corr}$) calculated according Eq. (3) were higher than those determined through the LPR technique as discussed in Section 3.1.2, as seen in Fig. 17. Similar to the LPR technique, EIS cannot provide information about $\beta_a$ and $\beta_c$. As a quick and non-destructive testing technique, EIS can still be taken as an important complementary approach as it provides information about $R_{ct}$ and $R_f$ which define the difficulty of kinetically controlled corrosion reactions.

**Table 2** EIS best-fit results (before pre-exposure to a DC current).

alt-text: Table 2

| | $R_s$(•cm2)Rf(•cm2)Cf(10 (Ω•cm$^2$) | $R_f$ (Ω•cm$^2$) | $C_f$ (10$^{-6}$S•s$^n$•cm$^{-2}$) | $n_f$ | $R_{ct}$(k•cm2)Cdl(10 (kΩ•cm$^2$) | | $C_{dl}$ (10$^{-6}$S•s$^n$•cm$^{-2}$) | $n_{dl}$ |
|---|---|---|---|---|---|---|---|---|
| 0.0 mol/L NaCl | 2.9 | 40.6 | 0.3 | 0.70 | 15.0 | −1.8 | 39.1 | 0.78 |
| | | | | | | +2.8 | | |
| 0.3 mol/L NaCl | 8.9 | 47.1 | 294.5 | 0.41 | 5.8 | −2.7 | 81.0 | 0.73 |
| | | | | | | +3.4 | | |
| 0.6 mol/L NaCl | 7.4 | 80.5 | 547.0 | 0.60 | 4.8 | −1.2 | 85.5 | 0.70 |
| | | | | | | +0.8 | | |
| 0.8 mol/L NaCl | 9.2 | 88.4 | 682.0 | 0.52 | 2.4 | −0.9 | 127.1 | 0.75 |
| | | | | | | +1.5 | | |

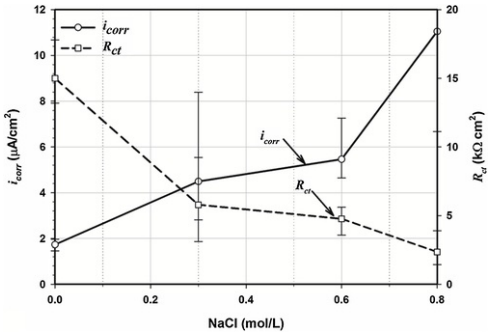


**Fig. 17** $i_{corr}$ determined based on EIS best-fit results.

(a) 0.0 M NaCl

(b) 0.3 M NaCl

~~(c) 0.6 M NaCl~~

~~(d) 0.8 M NaCl~~

alt-text: Fig. 17

Above three instrumental methods for electrochemistry allow for the determination of the corrosion current density ($i_{corr}$). Steel fibres demonstrated high resistance to chloride ions with 0.6 mol/L NaCl in the electrolyte. A comparison of these methods is shown in Table 3. In summary, Tafel polarization method is a preferred approach as it directly provides the corrosion density ($i_{corr}$) at equilibrium between the anodic and cathodic reactions (or a passive state). In addition, Tafel polarization provides useful kinetic information about $\beta_a$ and $\beta_c$ which cannot be determined by either the LPR or EIS technique. On the other hand, LPR and EIS techniques can still be taken as a useful complementary method for assessing the steel corrosion states due to its high efficiency and non-destructive nature.

**Table 3** Comparison of 3 methods for the determination of $i_{corr}$.

alt-text: Table 3

| | Cost | | Variation of $i_{corr}$ | Testing method |
|---|---|---|---|---|
| | Apparatus cost | Experimental time | | |
| Tafel polarization | High | ≤ 30 minutes | Low | Destructive |
| LPR | Low | ≤ 15 minutes | High | Non-destructive |
| EIS | High | ≤ 30 minutes* | High | Non-destructive |

* EIS scanning frequencies above $10^{-2}$ Hz.

Potential drop due to the current flowing through the electrolyte ($R_s$) may cause significant error in a kinetic model. This is of particular importance for the determination of $R_p$ through a LPR test. In this work, correction for $R_p$ was not considered due to the strong aqueous electrolyte used and this assumption was verified by the EIS best-fit results as seen in Table 2: $R_s$ was less than 10 Ω•cm$^2$.

### *3.1.4 CP polarization results*

In addition to above three approaches (i.e. Tafel polarization, LPR or EIS) for the determination of $i_{corr}$, cyclic potentiodynamic (CP) polarization was conducted to study the formation of the steel passivation layer and corrosion behaviour of steel fibres under a high positive overpotential which cannot be considered by above techniques. The CP polarization results are presented in Fig. 18. During the positive voltage scan, the electrode (steel) current density ($i$) remains almost constantly with an increase of the potential ($E$) which can be defined as a passivation potential, $E_{pass}$. $E_{pass}$ represents the potential value at which the passive layer is developed on the steel surface. The measured passivation current density ($i_{pass}$), which can be taken as a measure of the corrosion speed of steel in a passive state, was less than 1.5 μA/cm$^2$ under a chloride-free condition. With 0.8 mol/L NaCl, $i_{pass}$ was 4.5 μA/cm$^2$ which is still less than that of ordinary steel reinforcing bars in a passive state, i.e. 5 μA/cm$^2$ according to Edeleanu [39]. This result indicates that steel fibres have high corrosion resistance in a passive state, with and without NaCl in the electrolyte.

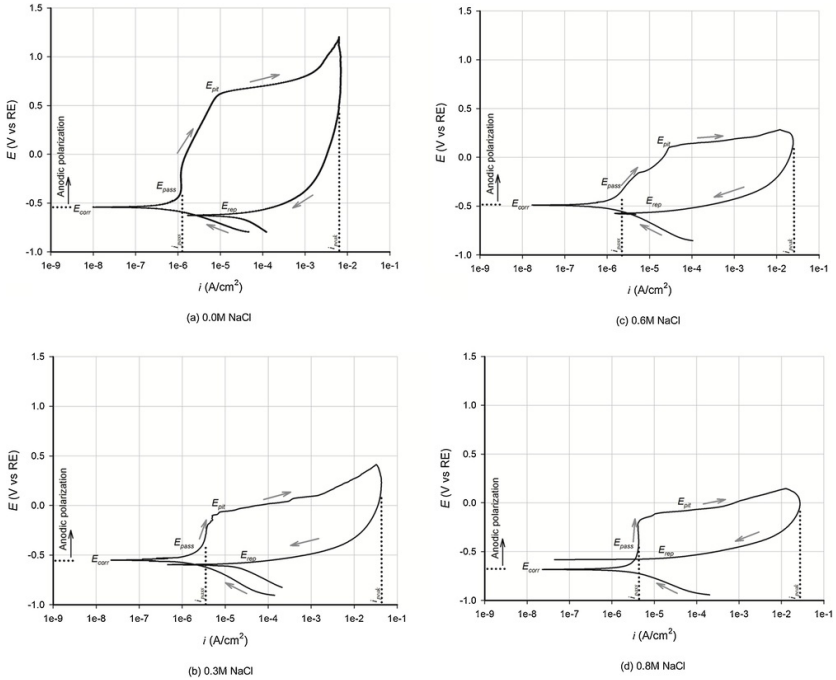


**Fig. 18** CP polarization results (before pre-exposure to a DC current).

alt-text: Fig. 18

With a further increase of $E$ ($\geq E_{pass}$), a gentle increase of $i$ was observed until the pitting potential ($E_{pit}$) was reached. $E_{pit}$ represents the DC voltage that breaks down the steel passive layer. $E_{pit}$ shifted from above 0.5 V (vs RE) under a chloride free condition to a negative value with a small amount of NaCl (i.e. 0.3 mol/L) in the electrolyte, indicating an earlier breakdown of the steel passive layer. This can be explained by the theory developed by Saremi and Mahallati [7]: the disruptive effect of chloride ions overcame the stabilizing effect of hydroxide ions in the electrolyte.

With a further increase of $E$ ($\geq E_{pit}$), $i$ increased significantly alongside serious steel anodic dissolution. A reverse scan was performed when a maximum positive voltage of 1.5 V (vs OCP) or a maximum current density of 30 mA/cm$^2$ was reached. The maximum current density was defined to prevent overloading the potentiostat. During the reverse voltage scan, the repassivation potential, $E_{rep}$, was identified. $E_{rep}$ was found to be close to $E_{corr}$, showing the steel passive layer was not repairable [7]. In addition to $E_{rep}$, the maximum current density $i_{peak}$ was observed during the reverse scan. $i_{peak}$ was only 7 mA/cm$^2$ under a chloride-free environment but it reached the maximum allowable value of 30 mA/cm$^2$ with only 0.3 mol/L NaCl in the electrolyte. This indicates that a small amount of chloride ions ($\leq$ 0.3 mol/L), which is insufficient to cause severe corrosion of steel fibres in a passive state ($E \leq E_{pass}$), still increases the risk of corrosion under a bigger external DC voltage as that experienced by a railway tunnel under a stray DC environment. More specifically, the normal increase of $i$ due to an increased DC voltage $E$, in presence of NaCl, to further increase of $i$ and this can be taken as a specific situation of stray DC-induced corrosion (i.e. an autocatalytic process) in nature. In summary, CP polarization provides additional useful information about the corrosion behaviour at an active state considering the combined effect of chloride and an external DC voltage which cannot be sufficiently investigated through Tafel polarization, LPR or EIS.

# 3.2 Corrosion behaviour of SFRC under a simulated stray DC environment

## *3.2.1 Corrosion behaviour of steel fibre in simulated concrete pore solutions*

An external DC voltage ($E$) allows the charged anions and cations in the electrolyte to flow throughout the bulk solution between the electrodes. It also provides the free energy required for an electrolytic cell to undergo coupled oxidizing-reducing reactions. Electron and ion transport developed in the electrolytic cell as discussed in Section 2.2.1 is shown in Fig. 19, along with possible anodic and cathodic reactions at the electrode-electrolyte interfaces. On the anode graphite surface, chloride oxidation to chlorine gas ( $2Cl^- \rightarrow Cl_2 + 2e^-$ ) would prevail in a chloride environment due to the slowly kinetically controlled half-cell reactions associated with $O_2$ evolution ( $4OH^- \rightarrow O_2 + 2H_2O + 4e^-$ ; $2H_2O \rightarrow O_2 + 4H^+ + 4e^-$ ). On the cathode graphite surface, $H_2O$

and $O_2$ reduction reactions ( $2H_2O + 2e^- \rightarrow H_2 + 2OH^-$ ; $O_2 + 2H_2O + 4e^- \rightarrow 4OH^-$ ) are both expected from an energetic point of view. However, the reduction of $O_2$ may be hindered due to the low solubility of $O_2$ in water, e.g. 285 µmol/L [40]. Dissolved $O_2$ can be further reduced due to the other chemical compounds e.g. NaCl and $Ca(OH)_2$, in the electrolyte [41].

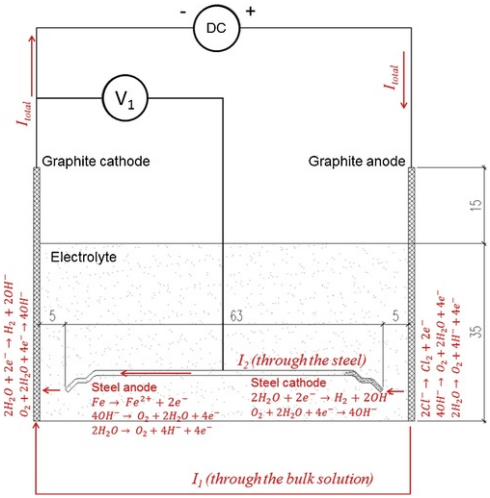


**Fig. 19** Possible electrochemical reactions involved in the stray DC interference test.

alt-text: Fig. 19

The potential difference between the electrode and the bulk solution induces the exchange of electrons and as such, an electric current is pushed through. In addition to this, a second pathway for electrons can be formed through the polarized steel fibre, as seen in Fig. 19. The side of the steel fibre adjacent to the graphite cathode is anodically (or positively) polarized, allowing the electrode potential to shift more positively. The other end of the steel fibre is cathodically polarized, allowing the electrode potential to shift more negatively. Steel corrosion occurs at its anodic side where the current leaves. At the steel cathode, the current flows from the electrolyte to the steel fibre, associated with the reduction reactions. Such a two-stream pathway is demonstrated as an equivalent electric circuit (Fig. 20) to model the steel-concrete interfacial electrochemical reactions. In this model, $R_1$ represents the resistance between the left graphite electrode and the steel fibre; $R_2$ represents the resistance between the right graphite electrode and the steel fibre; $R_3$ represents the bulk resistance between two graphite electrodes. The Faradaic current through the steel fibre (i.e. $I_2$) is a direct measure of the rate of the steel redox reactions. Given such quantitative analysis, $I_2$ is a strong function of $R_1$ and it can be determined according to Ohm's law ( $I_2 = \frac{V_1}{R_1}$ ).

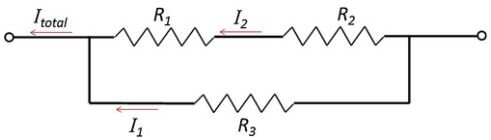


**Fig. 20** Equivalent circuit of the electrolytic cell shown in Fig. 19.

alt-text: Fig. 20

The measured voltage drop $V_1$ between the steel fibre and auxiliary graphite electrode is shown in Fig. 21. It indicates that $V_1$ increased with time in absence of NaCl, showing increased impedance and possible enhanced corrosion resistance which can be attributed to the development of steel passive layer under an alkaline condition. A combined effect of the DC current and 0.3 mol/L NaCl however led to a significant reduction in $V_1$, indicating reduced impedance along with enhanced corrosion reactions.

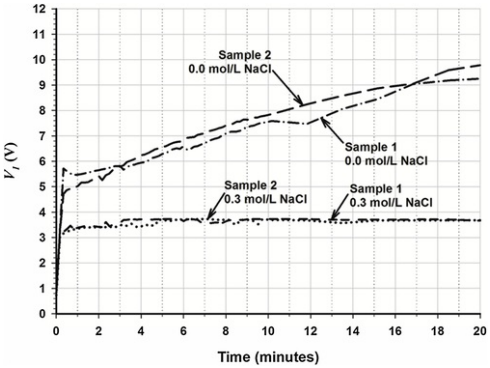


**Fig. 21** Voltage drop between steel and graphite electrode ($V_1$) – using simulated concrete pore solutions.

alt-text: Fig. 21

Under an external DC voltage, the steel anodic side shifts more positively (or anodically) and leads to the steel oxidation reaction as discussed. Ferrous hydroxide, $Fe(OH)_2$, is more favourable than bivalent $Fe^{2+}$ in an alkaline electrolyte [42]. $Fe(OH)_2$ can be further oxidized to form $Fe_2O_3$, resulting an oxide layer precipitated on the steel surface. Visual observation was conducted to assess the steel fibre surface after the stray DC interference test. Black corrosion product, rather than normal red dust ($Fe_2O_3$), was observed on the anodic side of the steel fibre after the simulated stray DC interference. This can be attributed to the formation of magnetite ($Fe_3O_4$) due to a deficiency of $O_2$ at the steel surface [13]. The chemical composition assessment of the corrosion product and its effects on the mechanical and durability performance of SFRC is an area where ongoing research is undertaken.

Fig. 22 shows the Tafel polarization results obtained after the stray DC interference test. $E_{corr}$ shifted to more negative values along with an increase of $i_{corr}$. With only 0.3 mol/L NaCl in the electrolyte, $i_{corr}$ was over 10 μA/cm$^2$ which is more than one order of magnitude higher than that obtained before the pre-exposure to the simulated stray DC environment (i.e. 0.5 μA/cm$^2$ as seen in Fig. 11 and Fig. 12), indicating serious steel corrosion. An increased corrosion intensity can be explained according to the parallel circuit model (Fig. 20): a larger percentage of the current always flows through the path of least resistance in a parallel circuit. Charge transfer resistance ($R_{ct}$) and membrane resistance ($R_f$) both reduce due to the presence of chloride ions (NaCl) in the electrolyte, just as depicted in Table 2. It leads to a reduction in $R_2$ and thus allows more electric current to flow through the path containing the steel fibre ($I_2$). As discussed, $I_2$ is a direct measure of the steel anodic dissolution speed and an increased $I_2$ allows more electrolytic currents to flow through the embedded steel fibre, leading to more serious corrosive attack. In summary, a small amount of chloride (≤ 0.3 mol/L), which in itself may not be sufficient to cause concerns of serious corrosion in SFRC, still increases the risk of stray DC induced corrosion.

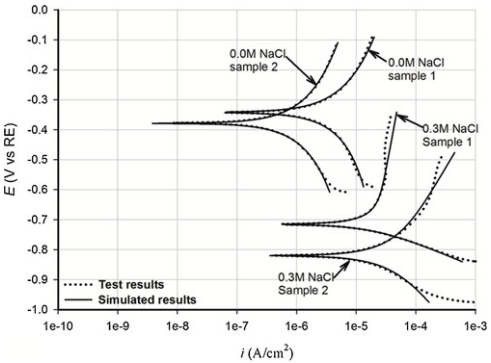


**Fig. 22** Tafel polarization test results after the 30-m DC interference.

alt-text: Fig. 22

## 3.2.2 Effect of solid electrolyte on the corrosion behaviour of steel fibres under a simulated stray DC environment

In order to verify that the results obtained using simulated concrete pore solutions were still applicable for SFRC, a 60-min stray DC interference test was conducted under a controlled DC current value of 30 mA. The measured voltage drop $V_1$ between the steel fibre and the auxiliary graphite electrode is shown in Fig. 23. It shows that the value of $V_1$ remained constantly during the simulated stray DC interference, showing that constant DC currents can be picked up and transferred by the steel

fibre. The $V_1$ obtained under a chloride-free environment was much higher than that with 2% NaCl (% by mass of cement), indicating greater impedance and possible enhanced corrosion resistance. This can be attributed to the high impedance of the solid electrolyte (i.e. mortar) without the presence of NaCl. Fig. 23 also shows that constant $V_1$ values were achieved during the polarization test, with and without the presence of NaCl, indicating a good protection provided by the steel passive layer.

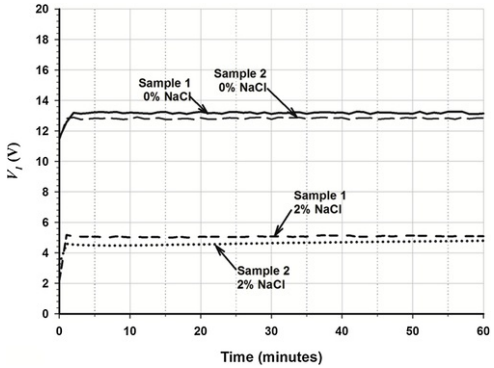


**Fig. 23** Voltage drop between steel and graphite electrode ($V_1$) – using SFRC as the solid electrolyte.

~~(a) Bode phase plot~~

~~(b) Bode $|Z|$ plot~~

~~(c) Nyquist plot~~

alt-text: Fig. 23

EIS was conducted after the simulated stray DC interference. EIS results are presented as the Bode plots (Fig. 24(a), (b)) and Nyquist plot (Fig. 24(c)). The Bode phase plot indicates that the phase angle ($\theta$) dropped constantly at low frequencies until the lowest value (valley) was reached at excitation frequencies ranging between 10 and 100 Hz, with and without added chlorides (NaCl). This indicates that a rust layer might have formed on the steel fibre surface and the speed of the corrosion reactions was affected by the diffusion speed through the rust layer [35]. The Bode $|Z|$ plot (Fig. 24(b)) also shows that total impedance, $|Z|$, reduced constantly from 15,000 Ω•cm$^2$ at an excitation frequency of 0.1 Hz to less than 2,000 Ω•cm$^2$ after the 1-hr DC interference even without the presence of NaCl, indicating enhanced stray current-induced corrosion. As the Bode plot is similar to that observed in Fig. 15, the same equivalent electronic circuit (Fig. 16) was used to represent the corrosion state experienced by the steel fibres after the stray DC interference test. EIS best-fit curves obtained from one sample based upon the equivalent electronic circuit modelling are shown in Fig. 24 and they match very well with the measured data. The EIS best-fit results obtained from two parallel samples in each group are shown in Table 4. $R_{ct}$ was 55.7 kΩ•cm$^2$ under a chloride free condition and it is much higher than that obtained under a similar condition but using an aqueous electrolyte, i.e. 15.0 kΩ•cm$^2$ as seen in Table 2. This shows the beneficiary effect of a solid electrolyte like mortar on the corrosion resistance of embedded steel and this finding agrees with Page [20]. On the other hand, a combined effect of NaCl and stray DC current accelerated the corrosion reactions at the steel-concrete interface: $R_{ct}$ reduced by two orders to 0.3 kΩ•cm$^2$ with 2% NaCl in mortar (% by mass of cement), showing high susceptibility for steel fibre corrosion. This can also be explained by the parallel circuit model as shown in Fig. 20. $R_{ct}$ forms a major part of the resistor $R_2$ in the equivalent electrical circuit (Fig. 20). The reduction in $R_{ct}$ due to the presence of NaCl led to an increase in $I_2$, or more stray current will be picked up by steel fibres in a chloride contaminated environment. In addition to $R_{ct}$, $C_{dl}$ increased significantly with 2% NaCl in the electrolyte, indicating that constant corrosion had occurred at the steel-concrete interface [14]. In summary, a small amount of NaCl (≤ 2% by mass of cement) increases the risk of stray DC current induced corrosion.

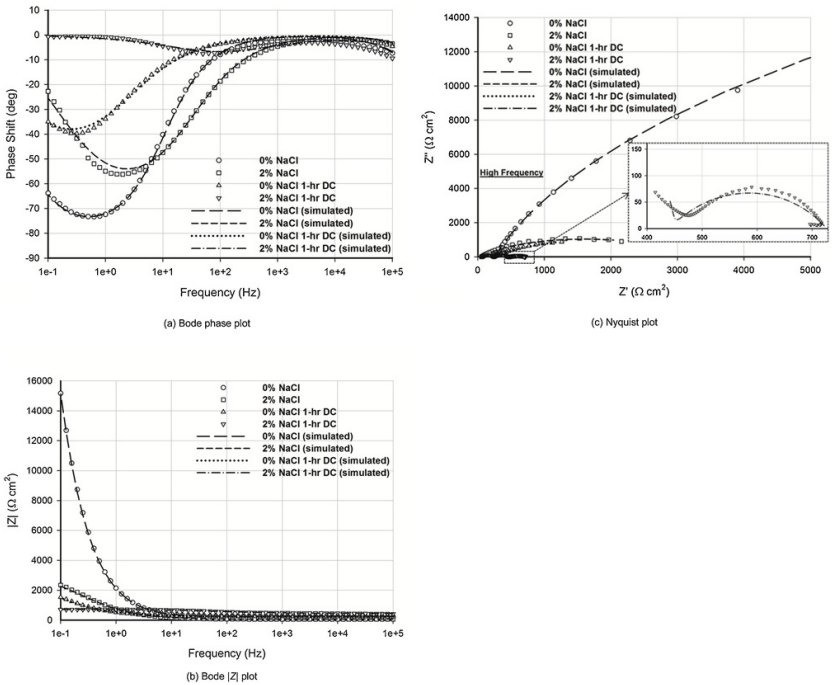


**Fig. 24** EIS data – SFRC before and after stray DC interference.

alt-text: Fig. 24

**Table 4** EIS best-fit results – SFRC before and after 1-hr stray DC interference.

alt-text: Table 4

| | $R_s$(•cm2)Rf(•cm2)Cf(10- (Ω•cm$^2$) | $R_f$ (Ω•cm$^2$) | $C_f$ (10$^{-9}$S•s$^n$•cm$^{-2}$) | $n_f$ | $R_{ct}$(k•cm2)Cdl(10- (kΩ•cm$^2$) | $C_{dl}$ (10$^{-6}$S•s$^n$•cm$^{-2}$) | $n_{dl}$ |
|---|---|---|---|---|---|---|---|
| 0% NaCl 0-hr | 10 | 248.1 | 3.1 | 0.90 | 55.7 ± 1.5 | 92.9 | 0.93 |
| 2% NaCl 0-hr | 7 | 59.2 | 1.4 | 0.99 | 3.1 ± 0.2 | 306.1 | 0.76 |
| 0% NaCl 1-hr | 8 | 193.8 | 0.6 | 0.99 | 3.6 ± 0.2 | 803.2 | 0.66 |
| 2% NaCl 1-hr | 6 | 443.5 | 0.4 | 0.99 | 0.3 ± 0.2 | 116.4 | 0.56 |

Fig. 24 (b), the Bode |*Z*| plot, shows a small |*Z*| at a high excitation frequency of $10^5$ Hz, indicating a small solution resistance ($R_s$). This was confirmed by the EIS best-fit results as seen in Table 4: $R_s$ was less than 10 Ω•cm$^2$. Fig. 24 (c) shows that impedance predicted through equivalent circuit modelling was less than the experimental data at high frequencies (e.g. up to $10^5$ Hz) when 2% NaCl was added into the mortar. This might be attributed to the formation of corrosion products on the steel surface due to the combined effect of stray currents and NaCl. This is an area where ongoing research including scanning electron microscope (SEM) analysis is undertaken. Results will be discussed in a separate paper.

After the stray DC interference test, SFRC samples were cut to expose the steel fibre sections at a distance of 1.5 cm from the centre of the steel fibre, as seen in Fig. 25; the boundary of corrosion products were highlighted with dashed lines. Serious corrosion of steel fibres was observed in SFRC containing 2% NaCl (by mass of cement) under the simulated stray DC environment. There was however no obvious sign of corrosion in the chloride-free SFRC sample after the pre-exposure to the simulated stray DC interference, indicating the mitigation effect of the solid electrolyte (i.e. mortar) used.

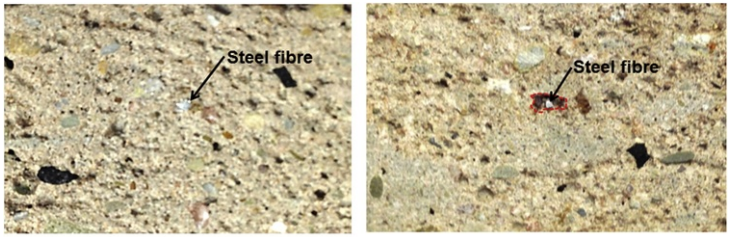


**Fig. 25** Section of SFRC after 1-hr stray DC interference.

~~(a) 0.0 mol/L NaCl~~

~~(b) 0.3 mol/L NaCl~~

alt-text: Fig. 25

## 3.3 BEM modelling of stray DC induced corrosion

The electric potential obtained through BEM modelling is presented as equipotential lines (or potential contour lines) (Fig. 26). The derived current densities in the model are presented as a vector plot and the magnitude is proportional to the length of the arrows. Distorted (noncylindrical) potential contour lines are observed between the graphite electrodes and steel fibres. This can be attributed to the small gap, i.e. 5 mm, between them [31]. When an electric current of 50 mA is passed through the graphite electrodes, the embedded steel fibres are polarized, allowing for a potential difference (or voltage drop) between them. The voltage drop ($V_1$) between the steel fibre and the auxiliary graphite electrode was 14.0 V under a chloride-free environment; a decreased voltage drop of 4.3 V was observed with 0.3 mol/L NaCl in the electrolyte. They were higher than those measured via the stray DC interference test as discussed in Section 3.2.1: $V_1$ was about 10 V under a chloride-free environment and reduced to 3.5 V with 0.3 mol/L NaCl in the electrolyte. This might be attributed to the electrolyte conductivities defined in the BEM model: they represented the aqueous electrolytes [32,33] but they may not sufficiently address the different electrical conductivity of the high density upholstery foam used in the stray DC interference test.

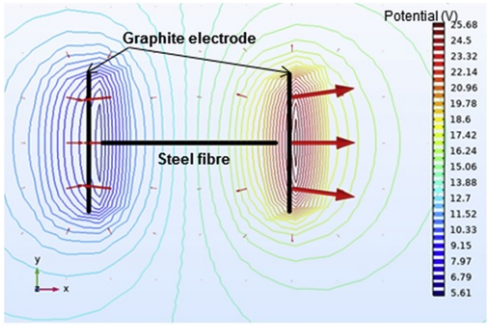


(a) 0.0 mol/L NaCl

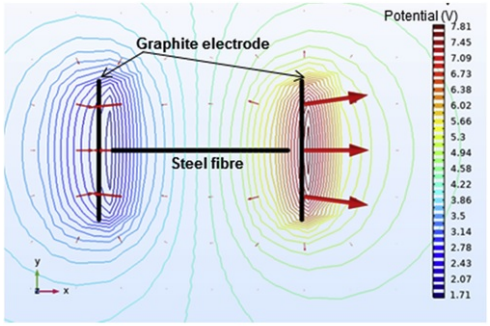


(b) 0.3 mol/L NaCl

**Fig. 26** BEM modelling result – equipotential lines and current density vectors.

alt-text: Fig. 26

The current densities developed in the steel fibre are presented in Fig. 27. It shows that the stray current can be discharged and picked up by the embedded steel fibre: the electrical current that enters the steel fibre provides protection; the electrical current that leaves the steel fibre leads to the loss of electrons and thus steel oxidation (corrosion) reactions, just as Fig. 19 depicts. The zero current density line was found to be approximately in the middle of the steel fibre. The presence of 0.3 mol/L NaCl in the electrolyte led to a decreased anodic and cathodic current density and this can be attributed to the increased conductivity of the electrolyte containing NaCl, allowing for more stray current ($I_{total}$) to flow through the electrolyte. This also verifies the assumption about the parallel circuit model (Fig. 20) which approximates the kinetics of the electrochemical reactions occurring at the steel-electrolyte interface. Table 4 indicates that $R_{ct}$ and $R_f$ reduce with time under a chloride condition, allowing more stray current to flow through the embedded steel fibre and lead to serious corrosion reactions. This effect however cannot be considered by the BEM modelling undertaken at a steady state. Transient modelling and analysis of such a dynamic process, which may pave the way for the development of a real-time SFRC (tunnelling) health monitoring system, is an area where ongoing research is being conducted.

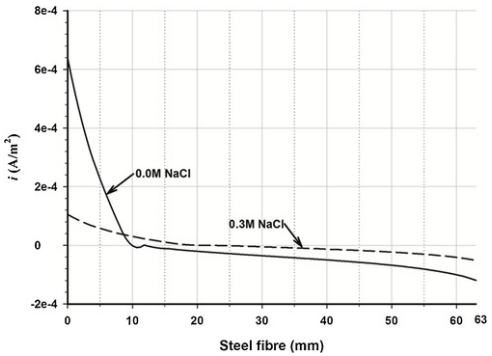


**Fig. 27** BEM modelling result – steel fibre current densities.

alt-text: Fig. 27

# 4 Conclusion

The corrosion resistance of steel fibres without a pre-exposure to a stray current environment was assessed through three instrumental methods for electrochemistry, i.e. Tafel polarization, linear polarization resistance (LPR), electrochemical impedance spectroscopy (EIS). Butler-Volmer regression analysis based on a Tafel polarization test is a preferred approach for the assessment of the corrosion resistance of steel fibres as it directly provides the corrosion density ($i_{corr}$) at equilibrium between the anodic and cathodic reactions. Steel fibre demonstrates high corrosion resistance even under a high chloride ion concentration condition (e.g. 0.6 mol/L).

Boundary element method (BEM) modelling, validated by the stray DC interference test results, indicates that discrete steel fibre can pick up and transfer stray DC current. CP polarization results indicate that the corrosion of steel fibres shows autocatalytic nature under the combined effect of an external DC voltage and chloride. A small amount of chloride ions in the concrete pore solution (≤ 0.3 mol/L), which is insufficient to cause severe corrosion of steel fibres in a passive state, still increases the risk of corrosion under an external DC voltage as that experienced by a railway tunnel under a stray DC environment. It should be noted that a solid electrolyte (e.g. concrete or mortar) has a beneficiary effect on the corrosion resistance of steel fibres although a high concentration of chloride ions (≥ 2% by mass of cement) still enhances the corrosion reactions by allowing more stray DC to flow through the embedded steel fibre.

# Acknowledgements

The author wishes to thank Lu for her patience and support over these years. The author gratefully acknowledges Colin Eddie, Stephen Wilkinson, John Booth and John Greenhalgh for their guidance and advice.

# References

**[1]** L. Bertolini, M. Carsana and P. Pedeferri, Corrosion behaviour of steel in concrete in the presence of stray current, *Corros~~ion Science~~. Sci.* **49**, 2007, 1056–1068.

**[2]** R. Kemp, Traction ~~energy m~~Energy Metrics, 2007, Rail Safety and Standards Board, Lancaster University; UK.

**[3]** ACI Committee 544, Report on the ~~physical properties and durability of fiber-reinforced c~~Physical Properties and Durability of Fiber-reinforced Concrete, 2010, American Concrete Institute; Farmington Hills, U.S.A..

**[4]** K. Tang, Stray current induced corrosion to steel fibre reinforced concrete, *Cem~~ent and Concrete Research~~. Concr. Res.* **100**, 2017, 445–456.

**[5]** K. Tang, Stray alternating current (AC) induced corrosion of steel fibre reinforced concrete, *Corros~~ion Science~~. Sci.* **152**, 2019, 153–171.

**[6]** A.M. Neville, Properties of ~~c~~Concrete, 2011, Pearson Education Limited; England.

**[7]** M. Saremi and E. Mahallati, A study on chloride-induced depassivation of mild steel in simulated concrete pore solution, *Cem~~ent and Concrete Research~~. Concr. Res.* **32**, 2002, 1915–1921.

**[8]** BRE, Digest 444, Part 3 Corrosion of ~~steel in concrete: investigation and a~~Steel in Concrete: Investigation and Assessment, 2000, BRE, Bracknell.

**[9]** P. Vassie, Reinforcement corrosion and the durability of concrete bridges, *Proc~~eedings of the Institution of Civil Engineers~~. Inst. Civ. Eng.* **76**, 1985, 1253–1256.

**[10]** D.A. Hausmann, Steel corrosion in concrete, *Materials protection* **6**, 1967, 19–23.

**[11]** P.S. Mangat and K. Gurusamy, Corrosion resistance of steel fibres in concrete under marine exposure, *Cem~~ent and Concrete Research~~. Concr. Res.* **18**, 1988, 44–54.

**[12]** A.M. Aguirre-Guerrero, R. Mejía-De-Gutiérrez and M.J.R. Montês-Correia, Corrosion performance of blended concretes exposed to different aggressive environments, *Constr~~uction and Building Materials~~. Build. Mater.* **121**, 2016, 704–716.

**[13]** Concrete Society, Technical Report 44 Relevance of ~~cracking in concrete to reinforcement c~~Cracking in Concrete to Reinforcement Corrosion, 2015, Concrete Society; Surrey, UK.

**[14]** C.Q. Ye, R.G. Hu, S.G. Dong, X.J. Zhang, R.Q. Hou, R.G. Du, C.J. Lin and J.S. Pan, EIS analysis on chloride-induced corrosion behavior of reinforcement steel in simulated carbonated concrete pore solutions, *j~~ournal of Electroanalytical Chemistry~~. Electroanal. Chem.* **688**, 2013, 275–281.

**[15]** M. Raupach and C. Dauberschmidt, Critical ~~Chloride Content for the Corrosion of Steel Fibres in Artificial Concrete Pore S~~chloride content for the corrosion of steel fibres in artificial concrete pore solutions, *International Concrete Abstracts Portal* **212**, 2003, 165–180.

**[16]** R.D. Moser, P.M. Singh, L.F. Kahn and K.E. Kurtis, Chloride-induced corrosion resistance of high-strength stainless steels in simulated alkaline and carbonated concrete pore solutions, *Corros~~ion Science~~. Sci.* **57**, 2012, 241–253.

**[17]** A. Poursaee, Corrosion of steel bars in saturated $Ca(OH)_2$ and concrete pore solution, *Concrete research letters* **1**, 2010, 90–97.

**[18]** J. Shi, W. Sun and G. Geng, Influence of carbonation on the corrosion performance of steel HRB335 in simulated concrete pore solution, *Jinshu Xuebao/Acta Metallurgica Sinica* **47**, 2011, 17–24.

**[19]** J. Shi, W. Sun, J. Jiang and Y. Zhang, Influence of chloride concentration and pre-passivation on the pitting corrosion resistance of low-alloy reinforcing steel in simulated concrete pore solution, *Constr~~uction and Building Materials~~. Build. Mater.* **111**, 2016, 805–813.

**[20]** C.L. Page, Initiation of chloride-induced corrosion of steel in concrete: ~~R~~role of the interfacial zone, *Mater~~ials and Corrosion~~. Corros.* **60**, 2009, 586–592.

**[21]** S. Patil, B. Karkare and S. Goyal, Corrosion induced damage detection of in-service RC slabs using acoustic emission technique, *Constr~~uction and Building Materials~~. Build. Mater.* **156**, 2017, 123–130.

**[22]** H. Sadeghi-Pouya, E. Ganjian, P. Claisse and K. Muthuramalingam, Corrosion durability of high performance steel fibre reinforced concrete, T.N. Peter Claisse, (Ed), Kyoto, Japan, *The 3rd ~~international conference on sustainable construction materials and t~~International Conference on Sustainable Construction Materials and Technologies* 2013.

**[23]** S.J. Duranceau, W.J. Johnson and R.J. Pfeiffer-Wilder, A study examining the effect of stray current on the integrity of continuous and discontinuous reinforcing bars, *Exp~~erimental Techniques~~. Tech.* **35**, 2011, 53–58.

**[24]** K. Wang, Q.S. Wu, M.C. Chen and L. Xie, Corrosion fatigue of reinforced concrete in the presence of stray current, 2011 International Conference on Electric Technology and Civil Engineering (ICETCE), 2011, 1133–1136.

**[25]** A. Yadav, Traction choices: overhead ac vs third rail dc, *International Railway Journal* 2013.

**[26]** C.A. Charalambous, I. Cotton, P. Aylott and N.D. Kokkinos, A ~~Holistic Stray Current Assessment of Bored Tunnel Sections of DC Transit SystemsIEEE Transactions on Power Delivery~~holistic stray current assessment of bored tunnel sections of DC transit systems, *Ieee Trans. Power Deliv.* **28**, 2013, 1048–1056.

**[27]** S. Laurens, P. Hénocq, N. Rouleau, F. Deby, E. Samson, J. Marchand and B. Bissonnette, Steady-state polarization response of chloride-induced macrocell corrosion systems in steel reinforced concrete — numerical and experimental investigations, *Cem~~ent and Concrete Research~~. Concr. Res.* **79**, 2016, 272–290.

**[28]** G. Cui, Z.-L. Li, C. Yang and M. Wang, The influence of DC stray current on pipeline corrosion, *Pet~~roleum Science~~. Sci.* **13**, 2016, 135–145.

**[29]** J. Wang, Analytical ~~e~~Electrochemistry, 2000, Wiley-VCH; New York, USA.

**[30]** A.O.S. Solgaard, M. Carsana, M.R. Geiker, A. Kuter and L. Bertolini, Experimental observations of stray current effects on steel fibres embedded in mortar, *Corros~~ion Science~~. Sci.* **74**, 2013, 1–12.

**[31]** L. Bortels, A. Dorochenko, B.Vd. Bossche, G. Weyns and J. Deconinck, Three-~~Dimensional Boundary Element Method and Finite Element Method Simulations Applied to Stray Current Interference Problems. A Unique Coupling Mechanism That Takes the Best of Both M~~dimensional boundary element method and finite element method simulations applied to stray current interference problems. A unique coupling mechanism that takes the best of both methods, *Corrosion* **63**, 2007, 561–576.

**[32]** S. K and N. TA, Influence of mixing vehicle on dissociation of calcium hydroxide in solution, *J. Endod.* **26**, 2000, 649–651.

**[33]** H. Golnabi, M.R. Matloob, M. Bahar and M. Sharifian, Investigation of electrical conductivity of different water liquids and electrolyte solutions, *~~Journal of theoretical and applied physics~~. Theor. Appl. Phys.* **3**, 2009, 24–28.

**[34]** Gamry, Gamry ~~Echem A~~echem analyst, Gamry Instruments, 2015, Inc..

**[35]** J. Wei, X.X. Fu, J.H. Dong and W. Ke, Corrosion evolution of reinforcing steel in concrete under dry/wet cyclic conditions contaminated with chloride, *~~Journal of Materials Science and Technology~~. Mater. Sci. Technol.* **28**, 2012, 905–912.

**[36]** C. Andrade and C. Alonso, Corrosion rate monitoring in the laboratory and on-site, *Constr~~uction and Building Materials~~. Build. Mater.* **10**, 1996, 315–328.

**[37]** M. Stern and A.L. Geary, Electrochemical polarization I. ~~a~~A theoretical analysis of the shape of polarization curves, *~~The Electrochemical Society~~Electrochem. Soc. Interface* **104**, 1957.

**[38]** H. Cesiulis, N. Tsyntsaru, A. Ramanavicius and G. Ragoisha, The ~~Study of Thin Films by Electrochemical Impedance S~~study of thin films by electrochemical impedance spectroscopy, In: I. Tiginyanu, P. Topala and V. Ursaki, (Eds.), *Nanostructures and Thin Films for Multifunctional Applications,* 2016, Springer International Publishing.

**[39]** C. Edeleanu, Corrosion control by anodic protection, *Platinum Metals Rev.* **4**, 1960, 86–91.

**[40]** P.R. Roberge, Corrosion ~~engineering: principles and p~~Engineering: Principles and Practice, 2008, McGraw-Hill.

**[41]** B.V. Lenntech, Oxygen (O) and ~~w~~Water, 2017.

**[42]** B. Popov, Corrosion ~~engineering: principles and solved p~~Engineering: Principles and Solved Problems, 2015, Elsevier Science Ltd.

## Queries and Answers

**Query:** Please check the presentation for the Tables 1–4, and correct if necessary.
**Answer:** All four tables (the contents in green) are correct.

**Query:** Please check that the affiliation link the author with correct departments, institutions, and locations, and correct if necessary.
**Answer:** The postcode should be UB8 3PH. This has been corrected in the context.

**Query:** Please confirm that the provided email “kangkangtang@gmail.com” is the correct address for official communication, else provide alternate e-mail address to replace the existing one, because private e-mail address should not be used in articles as the address for communication.
**Answer:** My Gmail is my research account and it is associated with the ORCID and ResearchGate. I will be grateful if it can be maintained as the primary contact email. If possible, I would like to add my University email address (kangkang.tang@brunel.ac.uk) alongside my Gmail. Thank you!

**Query:** The author names have been tagged as given names and surnames (surnames are highlighted in teal color). Please confirm if they have been identified correctly.
**Answer:** Yes. My name is shown properly.

**Query:** Please check the country name added in the affiliation, and correct if necessary.
**Answer:** Yes. This is correct.

**Query:** Please check the presentation for all the equations, and correct if necessary.

**Answer:** All equations have been checked and they are correct.

**Query:** Correctly acknowledging the primary funders and grant IDs of your research is important to ensure compliance with funder policies. We could not find any acknowledgement of funding sources in your text. Is this correct?

**Answer:** This project is not funded.

**Query:** Please provide volume number/issue number/page range for the Ref. [25].

**Answer:** "International Railway Journal" is published online (railjournal.com). Please use Feb as the volume, i.e.

A. Yadav, Traction choices: overhead ac vs third rail dc, *International Railway Journal.* **Feb**, 2013.